

Phase diagram of HgTe–ZnTe pseudobinary and density, heat capacity, and enthalpy of mixing of $\text{Hg}_{1-x}\text{Zn}_x\text{Te}$ pseudobinary melts

Ching-Hua Su, Yi-Gao Sha,^{a)} K. Mazuruk,^{a)} and S. L. Lehoczky
Space Science Laboratory, NASA Marshall Space Flight Center, Huntsville, Alabama 35812

(Received 29 November 1995; accepted for publication 21 March 1996)

In this article, the solidus temperatures of the $\text{Hg}_{1-x}\text{Zn}_x\text{Te}$ pseudobinary phase diagram for several compositions in the low x region were measured by differential thermal analysis and the HgTe–ZnTe pseudobinary phase diagram was constructed. The densities of two HgZnTe melts, $x=0.10$ and 0.16 , were determined by an *in situ* pycnometric technique in a transparent furnace over, respectively, 110 and 50 °C ranges of temperature. The thermodynamic properties of the melts, such as the heat capacity and enthalpy of mixing, were calculated for temperatures between the liquidus and 1500 °C by assuming an associated solution model for the liquid phase. [S0021-8979(96)02513-3]

I. INTRODUCTION

During the process of crystal growth of semiconductors from the melts, the thermodynamic and thermophysical properties of the melts are important parameters for growth process optimization as well as in the theoretical modeling of the process. However, in general, there exist only a limited amount of data¹⁻⁷ on the thermodynamic and thermophysical properties of the Hg-based molten semiconductors due to their high vapor pressures and chemical reactivity. The $\text{Hg}_{1-x}\text{Zn}_x\text{Te}$ ($0 \leq x \leq 1$) solid solutions have been studied⁸⁻²⁰ extensively in the low x ($x \leq 0.2$) region as a potentially superior material for the IR detector applications because the chemical bonding makes the material relatively more stable compared to HgCdTe. The only available thermodynamic data for this system are the pseudobinary liquidus and solidus curves for $x > 0.3$,^{21,22} a few liquidus points near the Te corner of the phase diagram,²³ and the partial pressures of Hg and Te_2 for various values of x .²⁴

This article describes the results for selected solidus temperatures determined by differential thermal analysis (DTA) and, together with previous data, provides a description of the HgTe–ZnTe pseudobinary phase diagram. In Sec. III, measured melt density variation with temperature is reported for two melt compositions. By assuming an associated solution model for the liquid phase, the thermodynamic properties of the HgZnTe melts were calculated and described in Sec. IV for interaction parameters obtained from an overall fit to the phase diagram and thermodynamic data. In general, the densities and the thermodynamic properties of the HgZnTe melts are in the same range and show similar trends as those of the HgCdTe melts. The evidence of HgZnTe solid solution being a superior material for the IR application compared to HgCdTe is not clear from these measured melt properties.

II. PSEUDOBI-NARY PHASE DIAGRAM

A. Sample preparation

The ampoules used in the measurements were made from fused silica tubing supplied by Heraeus Amersil, Inc.

The ampoules for low x ($x \leq 0.2$) $\text{Hg}_{1-x}\text{Zn}_x\text{Te}$ samples, corresponding to lower solidus and liquidus temperature ranges, and lower Hg pressures, were made from 12-mm-o.d. 8-mm-i.d. (12×8 mm) tubing whereas those for the high x ($x \geq 0.3$) samples were made from 14×8 mm tubing. After the ampoules were cleaned and outgassed in vacuum at 1010 °C for over 16 h, six-nine grade Zn and Te and seven-nine grade Hg provided by Johnson Matthey were loaded and the ampoules were sealed under vacuum. Excess Hg was added to compensate for the loss to the vapor phase. The composition and total weight for each ampoule are listed in Table I. The melting temperature of Sb contained in similar ampoules was used as reference. The amounts of 25–27 g six-nine-five grade Sb from Apache Chemicals were loaded into previously cleaned and outgassed ampoules made from either the 14×8 mm or 12×8 mm fused silica tubing. The HgZnTe ampoules were homogenized inside a rocking furnace using a specially designed heating schedule¹³ that utilizes the solid state diffusion process. The Sb ampoules were simply melted at 720 °C. Following sample casting, all the ampoules were then opened and resealed under vacuum to shorten the length to about 13 cm.

B. Experimental method for differential thermal analyses

The experimental apparatus for the DTA measurements is similar to that described previously,²⁵ except for the following modifications: (1) type S (Pt/Pt–10% Rh) thermocouples were used instead of type K (chromel–alumel) thermocouples, (2) the Inconel tube previously used in between the samples and the furnace was removed, and (3) the data were recorded and stored by a microcomputer. As in Ref. 25, the Sb ampoule, besides being the thermal capacity reference, also served as an internal thermocouple calibration reference. A series of heating rates, 1, 1.5, 2, 4 °C/min, were initially employed for a $\text{Hg}_{0.90}\text{Zn}_{0.10}\text{Te}$ sample to establish the optimum rate of 2 °C/min for the experimental arrangement. Sample inhomogeneities broaden the temperature range of phase transformation and, thus, introduce uncertainties into the transformation temperature deduced from the DTA signals. For this reason, the samples were always rap-

^{a)}Universities Space Research Association.

TABLE I. Compositions, excess Hg, and total weights of the DTA samples $\text{Hg}_{1-x}\text{Zn}_x\text{Te}$.

Sample	x	Excess Hg (g)	Total Weight (g)
DZ10	0.1002	0.4114	39.7456
DZ16	0.1586	0.3260	42.3574
DZ20	0.2001	0.0033	38.2699
DZ30	0.2998	-0.007	38.5011
DZ40	0.4001	0.0023	37.1281

idly solidified following casting and uniformly cooled after each DTA run. To improve alloy homogeneities, the samples were annealed at temperatures just below their solidus points before most of the runs as shown in Table II. To make a clear determination on the thermal arrest onset at the solidus temperature, the furnace was usually heated from 55 to 650 °C, cooled to 630 °C, held for 20 min and then heated again to temperatures between 790 and 880 °C, depending on the alloy composition. Several cooling curves were also measured and, similar to the previous DTA study on HgCdTe ,²⁵ thermal hysteresis in the form of 50–80 °C supercooling, depending on the cooling rate, for the HgZnTe samples and the Sb reference was observed. Therefore, only heating curves at the optimum rate of 2 °C/min were used for the determination of the thermal arrest onset. A typical DTA heating curve, showing the differential thermocouple voltage as a function of sample temperature, is plotted in Fig. 1. The melting point of Sb, serving as an internal thermal calibration, can be determined accurately. The solidus temperature of each sample was determined from the intersection of the initial part of the melting curve and the baseline extension. This measured solidus temperature was then corrected using a melting point of 630.5 °C for the Sb standard.

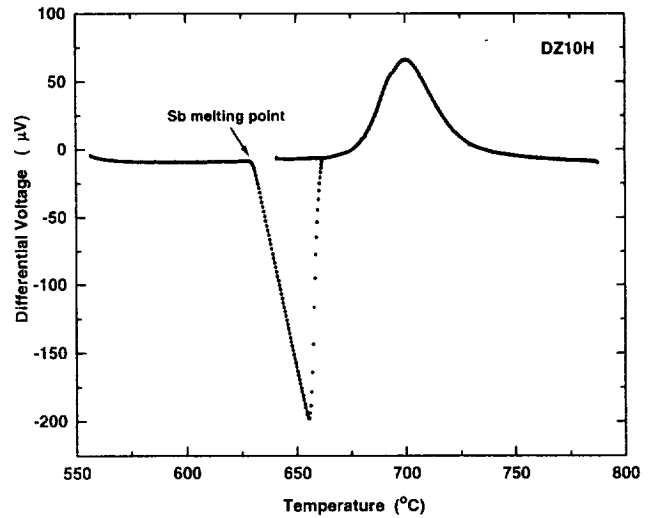


FIG. 1. Typical differential thermal analysis (DTA) data.

C. Results and discussion

Similar to the previous report on the $\text{Hg}_{1-x}\text{Cd}_x\text{Te}$ system,²⁵ the onset at the liquidus temperature was not clear for samples of small x ($x \leq 0.2$), as shown in Fig. 1. As for the high- x samples, the liquidus temperatures were too high so that the ampoules fractured from the high Hg partial pressures. Table II summarizes the annealing conditions, the heating rates, the measured Sb reference melting temperatures, the measured solidus temperatures, and the corrected solidus temperatures for all the samples.

The pseudobinary phase diagram of HgTe-ZnTe pseudobinary shown in Fig. 2 includes the data given in Table II as well as the liquidus and solidus temperatures previously reported.^{21,22} The present data agree well with

TABLE II. Summary of the solidus temperatures for HgZnTe samples in Table I.

Run	Heating rate (°C/min)	Measured Sb melting point in (°C)	Measured solidus temperature (°C)	Corrected solidus temperature (°C)
DZ10A	2	629.0	680.3	681.8
DZ10H ^a	2	630.4	679.9	680.0
DZ10I	2	630.8	678.8	678.5
				Average=680.1
DZ16A ^b	2	631.9	689.0	687.6
DZ16D	2	630.9	693.1	692.7
DZ16E	1	631.5	692.8	691.8
				Average=690.7
DZ20A ^c	2	630.2	683.3	683.6
DZ30C ^d	2	632.4	698.9	697.0
DZ30F ^d	2	641.7	708.0	696.8
				Average=696.9
DZ40B ^e	2	635.2	707.2	702.5

^aAnnealed at 660 °C for 2 days.

^bAnnealed at 670 °C for 3.8 days.

^cAnnealed at 670 °C for 5 days.

^dAnnealed at 670 °C for 10 days.

^eAnnealed at 675 °C for 7 days.

others and establish the low x region where no data were available before. The liquidus can be well fit by a straight line between the melting points of the end members, i.e., 670 °C for HgTe (Ref. 26) and 1290 °C for ZnTe (Ref. 27). The solidus curve can be fit, for practical purpose, by the polynomials

$$T_s \text{ (}^\circ\text{C)} = \begin{cases} 670.5 + 156.4x - 339.6x^2 + 521.3x^3 & \text{for } 0 < x < 0.79 \\ 342.1 + 2208.8x - 4285.1x^2 + 2894.2x^3 & \text{for } 0.79 < x < 0.96, \\ -80\,641.8 + 279\,213x - 319\,330x^2 & \\ + 122\,032x^3 & \\ \text{for } 0.96 < x < 1.0. \end{cases}$$

The above expressions for the liquidus and solidus temperatures agree well with the calculated results from a quantitative fit²⁸ to the diverse thermodynamic and phase diagram data for the Hg–Cd–Zn–Te quaternary system by assuming an associated solution model for the liquid phase.

DTA curves observed during cooling indicated considerable supercooling. For instance, a freezing temperature of 743 °C was observed during the cooling of the DZ20A cycle whereas the phase diagram indicates a liquidus temperature of 795 °C for an alloy composition of $x=0.20$.

There are several sources of error in the phase diagram data determined here. It is believed that the error in the thermocouple calibration was negligible because of the small temperature difference between the melting points of the Sb internal reference and the measured solidus temperatures. The uncertainties in the sample compositions, x , due to the loss of Hg are assumed to be negligible because of the small free volumes and the large masses. Although the shape of the solidus curve as a function of the stoichiometry, i.e., the metal to Te ratio, in the vicinity of y near 1/2 in $(\text{Hg}_{1-x}\text{Zn}_x)_{1-y}\text{Te}_y$ is not known, we assumed that the errors in the solidus temperatures associated with small deviations in y from 1/2 are negligible. Another uncertainty, probably the major source of error, is the subjectivity in selecting the proper phase transformation points from the DTA curves. The sharpness of the onset depends on the compositional

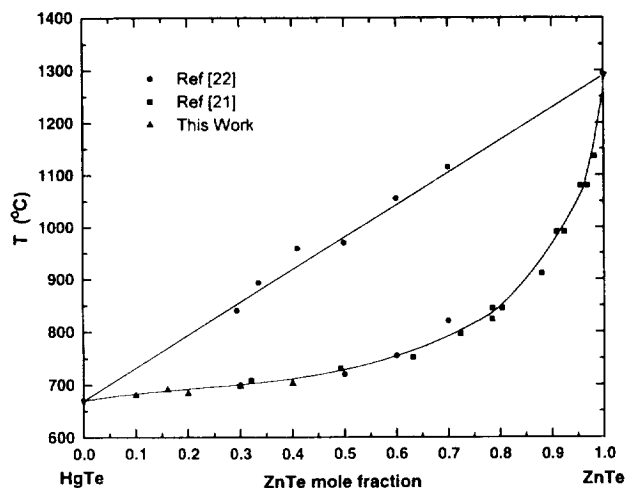


FIG. 2. Pseudobinary phase diagram of HgTe–ZnTe.

homogeneity of the sample and in the case of HgCdTe an annealing time of 15 h (Ref. 25) was adequate to result in a sharp transformation point. However, because of the lower solid state diffusivity of the HgZnTe than that of the HgCdTe (Ref. 18) even 4 days annealing was not long enough to show any significant difference in the sharpness of the onset. In general, this uncertainty was estimated to be about ± 2 °C.

III. DENSITY

A. Experiment

The densities of the HgZnTe melts were determined from the measurements of the meniscus height of the melts inside a transparent furnace by *in situ* visual observation. The thermometer-shaped ampoules were made from fused silica. The 15×9 mm “bulb” was 7–8 cm long and the stem that extended from the “bulb” was made from 6×3 mm fused silica tubing. The volume of the ampoule as a function of its height was measured by filling the ampoule with distilled water to various levels from a reference mark on the stem and measuring the corresponding weight of the ampoule in each case at room temperature. The value of 0.997 63 g/cm³ (Ref. 29) was used for the density of water at 22 °C. The effective cross section areas determined from the measurements correspond to the values of 3.015 mm and 3.189 mm for the diameters of the stem section of two ampoules used. The samples were prepared using the method described in Sec. II A. The total weight was 43.4822 g with 0.018 g excess Hg and 43.7654 g with 0.003 g excess Hg, respectively, for the Hg_{0.90}Zn_{0.10}Te and Hg_{0.84}Zn_{0.16}Te samples. The sample length in the stem region was 3 cm and 15 cm for $x=0.10$ and $x=0.16$, respectively.

The liquid level was visible inside the gold-plated transparent furnace and the separation between the meniscus and the reference mark was measured by a cathetometer with 0.05 mm resolution. During several measurements an air gap developed in the stem section and the levels of the meniscus for the air gap were measured. By subtracting the volume of the air gap, the total volume of the melt was obtained. Three calibrated thermocouples were strategically placed along the length of the ampoule for temperature measurements and a small positive vertical thermal gradient (hotter above) was maintained along the ampoule during the measurements.

B. Results and discussion

The densities of Hg_{0.84}Zn_{0.16}Te melts were measured in the temperature range of 795–850 °C. The high liquidus temperature and the associated high Hg pressure limited the measurements to a small temperature range of 50 °C. After four heating cycles between 790 and 850 °C the sample was equilibrated at 847 °C and the measurements were performed in an order of descending temperature. The width of the air gap was 7.8 mm at the highest temperature and shrank to 1.8 mm at the lowest temperature. Figure 3 shows the measured density for the Hg_{0.84}Zn_{0.16}Te melt which displays a slight increase of 0.6% from 797 to 847 °C and, for all practical purposes, can be treated as a constant of 7.476 g/cm³.

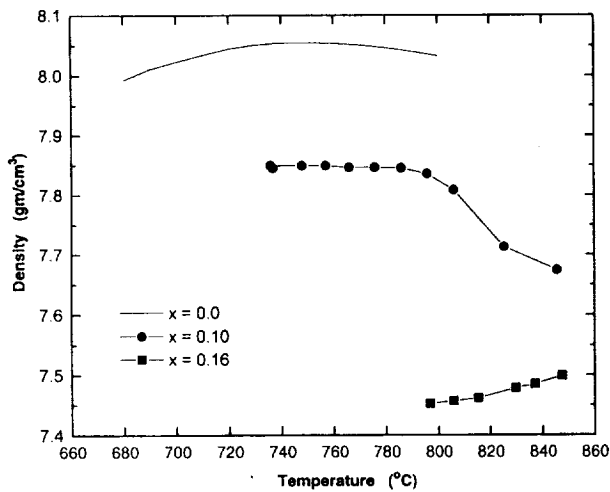


FIG. 3. Measured density of $\text{Hg}_{1-x}\text{Zn}_x\text{Te}$ melts.

As for the $\text{Hg}_{0.90}\text{Zn}_{0.10}\text{Te}$ melts, the densities were measured along a heating and cooling cycle. The measurements started from a temperature of 737°C to a maximum of 846°C and then back to 736°C . The heating and cooling data showed a hysteresis behavior with the largest discrepancy of $\pm 0.8\%$ at 795°C and almost no difference at 736°C . The density results for the cooling measurements are shown in Fig. 3, and are believed to be more reliable because of the longer equilibration time at higher temperatures. An air gap developed for the three highest temperature runs. The width of the air gap was 15.4 mm, 11.3 mm, and 1.3 mm for the measurements at 846°C , 833°C (not shown), and 825°C , respectively. The measured density of the $\text{Hg}_{0.90}\text{Zn}_{0.10}\text{Te}$ melt, despite of the hysteresis, decreases by 2.3%, from 7.85 g/cm^3 at 736°C to 7.67 g/cm^3 at 846°C in a temperature range of 110°C .

The measured density of the HgTe melt reported in Ref. 6 is also shown in Fig. 3. Similar to the HgCdTe system,⁶ the increasing ZnTe (or CdTe) content in the alloys results in a decrease in the density of the ternary melts. However, a maximum in the melt density away from the liquidus reported for the $\text{Hg}_{0.95}\text{Cd}_{0.05}\text{Te}$ and $\text{Hg}_{0.90}\text{Cd}_{0.10}\text{Te}$ melts⁶ was not observed here. The $\text{Hg}_{0.90}\text{Zn}_{0.10}\text{Te}$ melt displays the behavior of normal thermal expansion and the data for the $\text{Hg}_{0.84}\text{Zn}_{0.16}\text{Te}$ melt are essentially constant in the measured temperature range. The density of the solid solution at room temperature, derived from the lattice constant data,¹¹ is 7.8835 and 7.7584 g/cm^3 , respectively, for $\text{Hg}_{0.90}\text{Zn}_{0.10}\text{Te}$ and $\text{Hg}_{0.84}\text{Zn}_{0.16}\text{Te}$. Comparing these density values with those of the melts, the volume of a $\text{Hg}_{0.90}\text{Zn}_{0.10}\text{Te}$ sample maintains almost the same while that of a $\text{Hg}_{0.84}\text{Zn}_{0.16}\text{Te}$ sample contracts 4% from melt to solid at 25°C .

As for the hysteresis seen in the measured densities of the $\text{Hg}_{0.90}\text{Zn}_{0.10}\text{Te}$ sample, similar behavior was also reproducibly observed during viscosity measurements in the Hg-ZnTe melt.³⁰ Possible mechanisms for this observed phenomenon might be attributed to the macroscopic or microscopic inhomogeneities. The macroscopic inhomogeneity can be present, for instance, due to (1) insufficient mixing during material preparation, (2) small size bubbles for-

mation in the melt, or (3) evaporation/condensation of Hg into/from a free volume in the ampoule, which creates a thin boundary layer around the sample, thus modifying the wetting condition of the melt and changing the surface tension at the melt/free surface interface. The nature of the effect can also be microscopic. The subcritical clusters of the second phase³¹ or the formation of associated molecular species^{26,28} in the melt can be present in such a case. Any changes in the temperature will induce the redistribution in the cluster size and composition. This process is diffusion controlled and can be very slow.

The major error in the measured density of the melts is believed to come from the error in determining the liquid meniscus height. The shape of the meniscus was, most of the time, concave (toward the liquid) and an average, or effective, level was measured. For the ampoules used here (with an approximated melt volume of 5.9 cm^3) an error of 1 mm in the measured meniscus height results in an error of 0.12% in the measured volume and the corresponding error in density. The same error in the melt height would cause an error of about 0.25% in the measured density of HgCdTe for the ampoules used in Ref. 6, because of the larger i.d. of the stem section. The contribution from thermal expansion of the fused silica crucibles to the measured melt volumes was found to be negligible.

IV. HEAT CAPACITY AND ENTHALPY OF MIXING

A. Associated solution model

Thermodynamic properties, such as heat capacity and enthalpy of mixing, of HgZnTe pseudobinary melts cannot be easily determined experimentally, because of the limitations imposed by the high Hg partial vapor pressures. However, a fit²⁸ of the diverse thermodynamic and phase diagram data for the Hg-Cd-Zn-Te quaternary system by an associated solution model for the liquid phase was used to obtain good estimates. We also use this approach to establish thermodynamic properties for the melts of the Hg-Zn-Te ternary system. The detailed description of the model was described in Ref. 26. A brief summary of the model and the calculated results for the heat capacity and enthalpy of mixing in the pseudobinary melts are described below.

We assume that the liquid phase of HgZnTe consists of species Hg , Zn , Te , HgTe , and ZnTe , numbering consecutively as species 1–5, with mole fractions y_i , $i=1,\dots,5$. The thermodynamic components Hg , Zn , and Te are numbered consecutively 1–3 with atom fraction x_i , $i=1,2,3$. Mass balance leads to the following relations:

$$y_i = x_i(1 + y_4 + y_5) + [\delta(i,2) - 1]y_4 + [\delta(i,1) - 1]y_5, \quad (1)$$

$$i = 1, 2, 3,$$

where

$$\delta(i,j) = \begin{cases} 1 & \text{if } i=j \\ 0 & \text{if } i \neq j. \end{cases}$$

TABLE III. Interaction coefficients for Hg-Zn-Te system [Hg(1), Zn(2), Te(3), HgTe(4), ZnTe(5)] in calories per mole. (Note: 1 cal=4.184 J and T in K.) $\Delta G_4^0 = 10\,093.3 - 6.423\,78T$; $\Delta G_5^0 = 21\,151.7 - 3.253\,23T$.

	α_i	β_i
Hg-Zn	$\alpha_{12} = 176 + 0.436T$	$\beta_{12} = 0$
Hg-Te	$\alpha_{13} = -339.99 - 0.594\,874T$	$\beta_{13} = 942.498$
Hg-HgTe	$\alpha_{14} = 1916.31 - 0.317\,398T$	$\beta_{14} = 0$
Hg-ZnTe	$\alpha_{15} = 455.423 + 0.791\,065T$	$\beta_{15} = 0$
Zn-Te	$\alpha_{23} = 22\,744.4 - 15.965\,2T$	$\beta_{23} = -3245.99 + 0.408\,075T$
Zn-HgTe	$\alpha_{24} = 2350.9 - 8.519\,38T$	$\beta_{24} = 0$
Zn-ZnTe	$\alpha_{25} = 16\,850.3 - 9.094\,15T$	$\beta_{25} = -311.69 - 0.266\,161T$
Te-HgTe	$\alpha_{34} = 416.527 + 0.109593T$	$\beta_{34} = -314.842$
Te-ZnTe	$\alpha_{35} = 1752.27 - 0.852\,567T$	$\beta_{35} = -3.5129 + 0.666\,137T$
HgTe-ZnTe	$\alpha_{45} = 656.931 - 2.908\,17T$	$\beta_{45} = 0$

Independent of the specific form assumed for the excess Gibbs energy of mixing, one can obtain the following relations between the relative chemical potentials of species from solution thermodynamics²⁶

$$\bar{\mu}_4 = \bar{\mu}_1 + \bar{\mu}_3, \quad (2)$$

and

$$\bar{\mu}_5 = \bar{\mu}_2 + \bar{\mu}_3. \quad (3)$$

The thermodynamic description of the liquid phase is completed by assuming a functional form for the excess Gibbs energy of mixing from the liquid elements:

$$\Delta G_m^{xs} = \sum_{i=1}^5 \sum_{j=1}^5 (\alpha_{ij} + \beta_{ij}y_j)y_i y_j - y_4 \Delta G_4^0 - y_5 \Delta G_5^0, \quad (4)$$

where $\alpha_{ij} = \alpha_{ji}$, $\alpha_{jj} = 0$, and $\beta_{ij} = -\beta_{ji}$. The α_i and β_i are composition-independent interaction coefficients that are the adjustable parameters of the model along with the Gibbs energy of dissociation of the molecular species, ΔG_4^0 and ΔG_5^0 . The relative excess chemical potential of species p can be derived from Eq. (4) and is given by

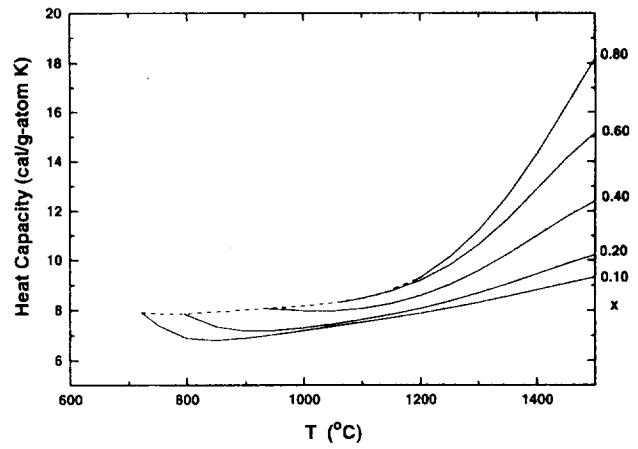


FIG. 5. Calculated heat capacity for $Hg_{1-x}Zn_xTe$ melts. (Note: 1 cal/cm = 4.184 W/cm K)

$$\begin{aligned} \bar{\mu}_p^{xs} = & 2 \sum_{i=1}^5 \left[\alpha_{ip} + \left(\frac{y_i}{2} - y_p \right) \beta_{pi} \right] y_i \\ & - \sum_{i=1}^5 \sum_{j=1}^5 (\alpha_{ij} + 2\beta_{ij}y_j)y_i y_j - \delta(p,4)\Delta G_4^0 \\ & - \delta(p,5)\Delta G_5^0. \end{aligned} \quad (5)$$

Once the thermodynamic model has been defined the thermodynamic properties of the melts can be derived using basic thermodynamic equations. The relative partial molar enthalpies and entropies of the species are related to the corresponding relative chemical potentials by the thermodynamic equations

$$\bar{h}_i = \left(\frac{\partial}{\partial (1/T)} (\bar{\mu}_i/T) \right)_{y_k} \quad (6)$$

and

$$\bar{S}_i = - \left(\frac{\partial \bar{\mu}_i}{\partial T} \right)_{y_k}, \quad i = 1, \dots, 5. \quad (7)$$

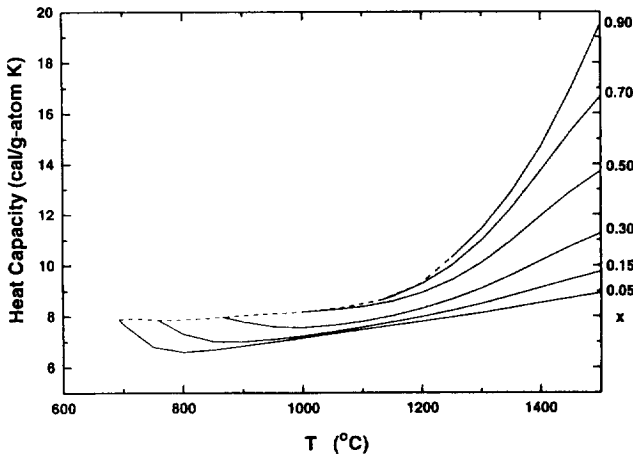


FIG. 4. Calculated heat capacity for $Hg_{1-x}Zn_xTe$ melts. (Note: 1 cal/cm = 4.184 W/cm K.)

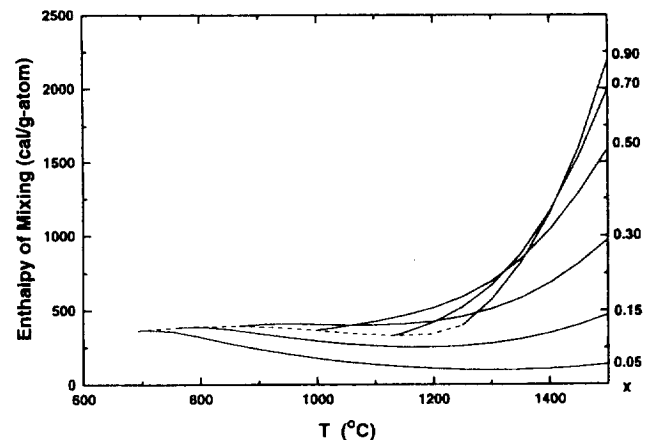


FIG. 6. Calculated enthalpy of mixing for $Hg_{1-x}Zn_xTe$ melts. (Note: 1 cal=4.184 J.)

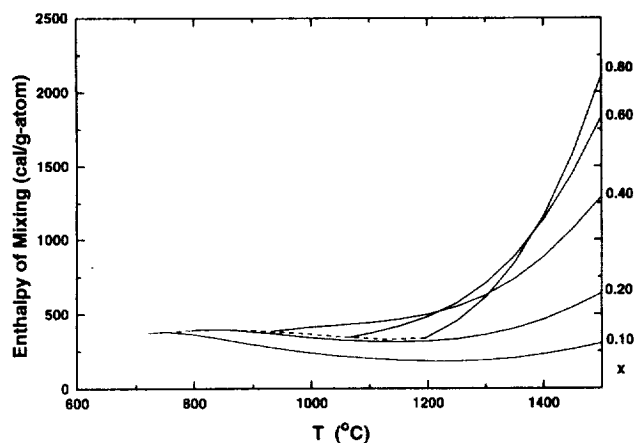


FIG. 7. Calculated enthalpy of mixing for $\text{Hg}_{1-x}\text{Zn}_x\text{Te}$ melts. (Note: 1 cal=4.184 J.)

The enthalpy and entropy of mixing per mole of species are given by

$$Z_m = \sum_{i=1}^5 y_i \bar{Z}_i, \quad (8)$$

where Z denotes either enthalpy or entropy. These properties can be further converted to the corresponding quantities per gram-atomic weight of components to provide a comparison with the experimental results by the relation

$$\Delta Z_m^{\text{g atom}} = \frac{\Delta Z_m}{(1 + y_4 + y_5)}. \quad (9)$$

The constant pressure relative heat capacity is defined as

$$\Delta C_p^{\text{g atom}} = (\partial \Delta H_m^{\text{g atom}}) / (\partial T)_{x_1, x_2, p}, \quad (10)$$

and is the difference between the heat capacity of the solution and the sum of the unmixed liquid elements. Once the relative heat capacity is calculated by means of Eqs. (8)–(10), the heat capacity of the melt can be determined from the following expression:

$$C_p^{\text{g atom}} = \Delta C_p^{\text{g atom}} + x_1 C_{p1}^l + x_2 C_{p2}^l + x_3 C_{p3}^l, \quad (11)$$

where C_{p1}^l , C_{p2}^l , and C_{p3}^l are the heat capacities of the pure liquid elements, Hg, Zn, and Te, respectively, and the values used are 6.61, 7.5, and 7.874 cal/g atom K, respectively.

B. Results and discussion

As given in Ref. 28, the interaction parameters were determined by a simultaneous fit to the diverse and extended phase diagram and thermodynamic data for the Hg–Cd–Zn–Te system. The set of parameters pertaining to the Hg–Zn–Te system is tabulated in Table III. The values of the heat capacity for various pseudobinary melts at temperatures between the corresponding liquidus temperatures and 1500 °C are summarized in Figs. 4 and 5. The dotted lines connect the data points along the liquidus temperatures.

The magnitude and the trend of the calculated values are similar to that of the HgCdTe melts reported in Ref. 32 for temperatures between 670 and 1100 °C. When the temperature gets above 1100 °C, the calculated heat capacity values for the HgZnTe melts increase monotonically with increasing temperature and reach above 19 cal/g atom K at 1500 °C for $\text{Hg}_{0.10}\text{Zn}_{0.90}\text{Te}$. The calculated enthalpies of mixing are given in Figs. 6 and 7.

ACKNOWLEDGMENTS

The authors appreciate the technical assistance of C. Bahr, R. Ross, and D. Lovell. The work was supported by the Microgravity Science and Applications Division of the National Aeronautics and Space Administration.

- ¹ V. M. Glazov, S. N. Chizhevskaya, and N. N. Glagoleva, *Liquid Semiconductors* (Plenum, New York, 1969).
- ² A. R. Regel, I. A. Smirnov, and E. V. Shadrachev, *Phys. Status Solidi* **5**, 13 (1971).
- ³ B. J. Keene, *Surf. Interface Anal.* **10**, 367 (1987).
- ⁴ S. Nakamura and T. Hibiya, *Int. J. Thermophys.* **13**, 1061 (1992).
- ⁵ L. R. Holland and R. E. Taylor, *J. Vac. Sci. Technol. A* **1**, 1615 (1983).
- ⁶ D. Chandra and L. R. Holland, *J. Vac. Sci. Technol. A* **1**, 1620 (1983).
- ⁷ H. Maleki and L. R. Holland, *J. Appl. Phys.* **76**, 4022 (1994).
- ⁸ M. C. Petty and C. Juhasz, *J. Phys. D* **9**, 1605 (1976).
- ⁹ Aden. Sher, A.-B. Chen, W. E. Spicer, and C.-K. Shih, *J. Vac. Sci. Technol. A* **3**, 105 (1985).
- ¹⁰ Ariel. Sher, D. Eger, A. Zemel, H. Feldstein, and A. Raizman, *J. Cryst. Growth* **72**, 108 (1985).
- ¹¹ Ariel. Sher, D. Eger, A. Zemel, H. Feldstein, and A. Raizman, *J. Vac. Sci. Technol. A* **4**, 2024 (1986).
- ¹² R. Triboulet, A. Lasbley, B. Toulouse, and R. Granger, *J. Cryst. Growth* **79**, 695 (1986).
- ¹³ C.-H. Su, S. L. Lehoczky, and F. R. Szofran, *J. Cryst. Growth* **86**, 87 (1988).
- ¹⁴ M. Schenk and A. Fissel, *J. Cryst. Growth* **86**, 502 (1988).
- ¹⁵ R. N. Andrews, S. D. Walck, M. W. Price, F. R. Szofran, C.-H. Su, and S. L. Lehoczky, *J. Cryst. Growth* **99**, 717 (1990).
- ¹⁶ R. Granger, A. Lasbley, A. Seyni, S. Rolland, and R. Triboulet, *J. Cryst. Growth* **101**, 241 (1990).
- ¹⁷ Ariel. Sher, A. Tsigelman, E. Weiss, and N. Mainzer, *J. Vac. Sci. Technol. A* **8**, 1093 (1990).
- ¹⁸ S. Fang, L. J. Farthing, M.-F. S. Tang, and D. A. Stevenson, *J. Vac. Sci. Technol. A* **8**, 1120 (1990).
- ¹⁹ M. P. Volz, F. R. Szofran, S. L. Lehoczky, and C.-H. Su, *Solid State Commun.* **75**, 943 (1990).
- ²⁰ S. N. Ekpenuma and C. W. Myles, *J. Vac. Sci. Technol. A* **10**, 208 (1992).
- ²¹ J. C. Wooley and B. Ray, *J. Phys. Chem. Solids* **13**, 151 (1960).
- ²² E. Cruceanu, D. Niculescu, N. Nistor, and Al. Aldea, *Rev. Roum. Phys.* **9**, 499 (1964).
- ²³ E. J. Smith *et al.* *J. Vac. Sci. Technol. A* **5**, 3043 (1987).
- ²⁴ K.-T. Chen, Y.-G. Sha, and R. F. Brebrick, *J. Vac. Sci. Technol. A* **8**, 1086 (1990).
- ²⁵ F. R. Szofran and S. L. Lehoczky, *J. Electron. Mater.* **10**, 1131 (1981).
- ²⁶ R. F. Brebrick, C.-H. Su, and P.-K. Liao, in *Semiconductors and Semimetals*, edited by R. K. Willardson and A. C. Beer (Academic, New York, 1983), Vol. 19, Chap. 3.
- ²⁷ B. M. Kulwicki, Ph.D. thesis, University of Michigan, 1963.
- ²⁸ T.-C. Yu and R. F. Brebrick, *J. Phase Equilib.* **13**, 476 (1992).
- ²⁹ H. A. Bowman, R. M. Schooner, and M. W. Jones, *J. Res. Nat. Bur. Stand. (U.S.)* **71C**, 179 (1967).
- ³⁰ K. Mazuruk, C.-H. Su, Y.-G. Sha, and S. L. Lehoczky, *J. Appl. Phys.* (to be published).
- ³¹ V. I. Yukalov, *Phys. Rep.* **208**, 395 (1991).
- ³² C.-H. Su, *J. Cryst. Growth* **78**, 51 (1986).